Materials Science and Engineering A 550 (2012) 342–349

Contents lists available at SciVerse ScienceDirect

Materials Science and Engineering A

journal homepage: www.elsevier.com/locate/msea

Finite element investigation of size effects on the mechanical behavior of nickel single crystals

C. Keller[a,*], A.M. Habraken[b], L. Duchene[b]

[a] Ermeca-GPM, UMR 6634 CNRS, Université de Rouen, INSA de Rouen, Avenue de l'Université, 76800 Saint-Etienne du Rouvray, France
[b] Department ArGEnCo, Division MSF, University of Liege, Chemin des Chevreuils 1, 4000 Liege, Belgium

ARTICLE INFO

Article history:
Received 19 March 2012
Received in revised form 19 April 2012
Accepted 24 April 2012
Available online 3 May 2012

Keywords:
Finite element method
Crystal plasticity
Size effects
Single crystal
Boundary conditions

ABSTRACT

The influence of dimensions on the mechanical behavior of f.c.c. single crystals with dimensions larger than a few micrometers has been the topic of many experimental investigations and controversies during the 1970s and this question is still open. The objective of this article is to shed new light on this point by performing finite element simulations thanks to a strain gradient crystal plasticity model. Based on the model identification for nickel, several single crystal samples with various thicknesses and orientations were tested numerically in tension. The effect of dimensions was then analyzed considering the spatial distribution of dislocation densities. Near loading boundaries, dislocation density gradients appeared perpendicular to the Burgers vector direction of the primary activated slip system which modified the mechanical behavior. These gradients are discussed in terms of boundary conditions, crystal orientation and dislocation interactions with surfaces.

1. Introduction

The last decades have been marked by a considerable effort made by the mechanic of materials community to understand the mechanical behavior of metallic materials at small scales. This effort has been motivated by the strong trend of miniaturization dedicated to the micro devices which are of great economical importance. Due to the reduced dimensions of these micro-systems, metallic parts with dimensions typically between 0.5 μm and 100 μm are employed. For these components, the size of the microstructure is generally no longer negligible with respect to the dimensions and size effects occur, which modify the mechanical properties. The design and the metal forming of micro-parts, when size effects are not properly considered, may be erroneous, resulting in several problems such as low reliability or high production costs [1].

These size effects can be classified into four classes. The statistical effect (i.) appears when the length scale characteristic of the microstructure is close to the sample dimensions. In this case, the samples cannot be considered as a representative volume element and the mechanical behavior is generally weaker due to material stiffness inhomogeneities. For polycrystals, this phenomenon is linked to the low number of grains inside the cross section which leads to strong stress gradients [2–5].

The surface effects (ii.) appear when the surface over volume ratio becomes significant. In this case, the surface regions, which behave differently due to their proximity with the solid boundaries, dominate the global response of the specimen. For samples with dimensions larger than a few hundred microns, the influence of surface effects has been widely studied experimentally for Al and Cu single crystals during the 1970s. Two different phenomena were reported depending on the material: a softening of the behavior for Cu single crystals oriented for single glide [6–9] and a hardening for Al [10–13]. Following Basinski [14] and Nabarro [15], this discrepancy can be explained by an oxide layer formation for Al which prevents the dislocations to escape through the crystal surface. These surface effects also seem to depend on the crystallographic orientation of the single crystals. For Cu samples oriented for multiple glide, no surface effects appeared compared to single glide orientation [16]. From a macroscopic point of view, these surface effects seem to modify the hardening stages with an increase in stage I extent for small dimension specimens [6]. Moreover, dislocation sources on surfaces may lead to a preferential hardening of the surface regions for micro-sized samples [17].

The third size effect (iii.) is attributed to strain gradients occurring for instance during bending, nano-indentation or tension of coated thin films [18–21]. In these cases, inhomogeneous plastic deformation occurs involving the evolution of Geometrically Necessary Dislocations (GNDs) which are more important for thinner specimens. The last size effect (iv.) is suggested for nanometer sized samples when dimensions are in the range of individual dislocation segments. In this respect, several models were proposed such as the

* Corresponding author. Tel.: +33 232959865; fax: +33 232959704.

0921-5093/$ – see front matter © 2012 Elsevier B.V. All rights reserved.
http://dx.doi.org/10.1016/j.msea.2012.04.085

starvation model or the troncature model [22,23]. In this case, only few dislocations are available to carry the plastic deformation due to their strong interactions with free surfaces leading to the famous "smaller is stronger" effect.

These size effects involve two different trends depending on the dimension range. From macro specimens to micro-sized specimens, a "smaller is softer" trend (i. and ii. size effects) is generally observed while the following transition from micro to nano leads to a "smaller is stronger" effect widely characterized for micropillars and thin films (iii. and iv. size effects) [24–26]. If the "smaller is stronger effect" was considerably investigated, some aspects of the "smaller is softer" phenomenon such as the effect of dimensions on the single crystal behavior remain unclear and must be analyzed in order to understand the effect of the dimensions for all scale ranges.

Experimentally, performing mechanical tests with small single crystals is difficult due to the handling of the samples. Finite Element simulation (FE) is then an alternative tool to study the effect of miniaturization. Such FE simulations require models able to correctly reproduce both surface effects and strain gradients. Among these models, the strain gradient crystal plasticity ones are convenient due to the introduction of a plasticity length scale and the modeling of the GNDs when surfaces are either completely free or completely passivated with respect to the escape of dislocations.

This work is hence focused on the investigation of the effects of the dimensions for single crystals with dimensions ranging from micro to macro scales. The objective is to clearly understand the effect of the sample dimensions on the stress and dislocation density distributions as a function of the crystal orientation. Tensile test simulations are hence performed using a strain gradient crystalline plasticity model identified for nickel. This material, which presents similar deformation mechanism as Al and Cu, was not involved in the experimental discrepancy cited above and may allow us to draw new conclusions. The macroscopic response together with the spatial distribution of dislocation densities and slip system activities are studied as a function of dimensions, crystal orientation and free or passivated surfaces. The results show that the effect of dimensions on the mechanical behavior strongly depends on boundary conditions.

2. Simulations

2.1. Model

The strain gradient plasticity model used in this study proceeds from the work of Evers et al. [27,28]. The key feature of the model is the incorporation of both GND accommodating strain gradients and Statistically Stored Dislocation (SSD) associated to the slip resistance. For the sake of conciseness with respect to the complexity of the model, its complete description with the different constitutive equations can be found in the literature [27,28,5]. It can be noticed that this model involves 21 degrees of freedom at FE nodes (3 displacements and 18 GND densities) and that simulations are highly time consuming. Moreover, 25 material parameters are necessary for the model which needs a specific identification procedure.

2.2. Mesh and boundary conditions

Due to the long computation time, a simplified mesh was employed for the simulations. All the samples, regardless of their dimensions, were meshed with 500 quadratic elements consisting on 20 nodes and 8 gauss points. Such a mesh ensures a good accuracy as revealed by a mesh sensitivity analysis. Fig. 1(a) illustrates this mesh in 3D together with the boundary conditions. These latter were chosen according to the experimental tensile tests extracted from the literature results used to identify the model. These

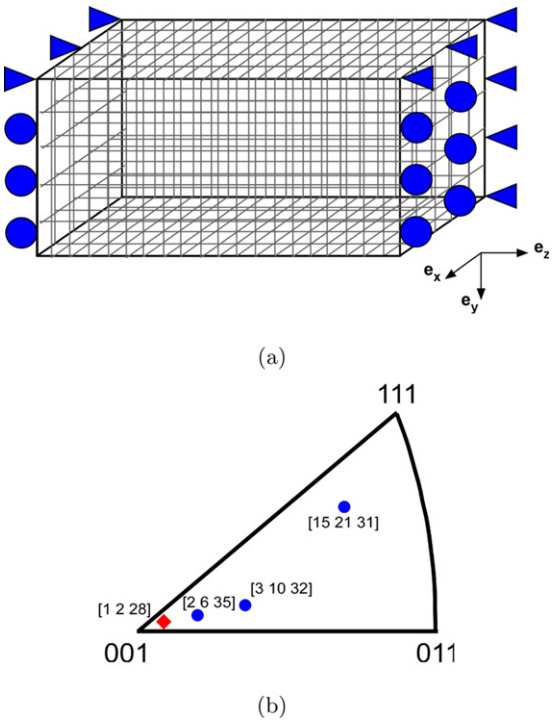

Fig. 1. (a) 3D illustration of the mesh and boundary conditions for the simulated tensile tests; (b) crystal orientations used for identification of the strain gradient crystalline plasticity model for Ni. (For interpretation of the references to color in the text, the reader is referred to the web version of the article.)

boundary conditions correspond to conventional tensile tests. On loading surfaces, displacements along $\mathbf{e}_x$ and $\mathbf{e}_y$ are free and GND can develop (dislocations are prevented to escape from loading surfaces). On the lateral surfaces, GND densities are restrained to 0 to fulfill free surface conditions, or let free to reproduce the effect of a hard layer on surfaces.

2.3. Identification

So far, crystalline plasticity models have been widely identified and applied for Cu and Al single crystals and polycrystals [29,30,27]. In the author's knowledge, no identification of this model for nickel has been reported. A specific parameters identification was then achieved for this material by comparisons between simulated and experimental tensile curves of single crystals with different crystallographic orientations. These different crystal orientations allow us to identify different model parameters thanks to the different hardening mechanisms associated to the activated slip systems. Compared to Cu and Al, experimental tensile tests of pure Ni single crystals are scarce in the literature. Among the available references [31–40] some of the results cannot be used for the identification because of the lack of experimental details such as sample dimensions, the accurate orientation or the tensile conditions (strain rate and boundary conditions). The parameter identification was hence achieved using the work of Hecker et al. [35] and Venkatesan et al. [40] which are well documented. Three single glide orientations and a multiple glide case were extracted from these two articles. Fig. 1(b) illustrates the orientations in the standard triangle of the crystals extracted from the work of Hecker et al. [35] (orientation [1 2 28], red rhomb) and from the work of Venkatesan et al. [40] (blue circles).

Due to the long computation time, no automatic procedure was possible to identify the parameters for Ni. As a consequence, a manual multi-step procedure was carried out to correctly identify the model parameters. Among the 25 parameters, the Burgers vector

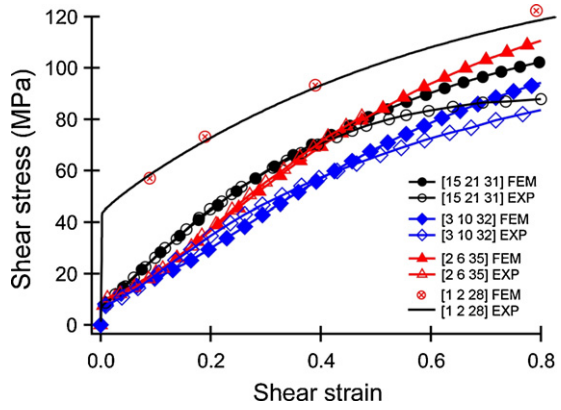

Fig. 2. Comparisons between experimental tensile tests proceeding from the literature and simulation predictions. For each simulation, the shear stress was obtained by multiplying the tensile flow stress with the maximal Schmid factor of the slip systems as done for the experimental curves in the literature.

b, the elastic coefficients C_{ij} and the immobilization matrix coefficients $\mathbf{H}_{ij}$ were identified by means of a literature review. In a first step of the identification, the model was integrated analytically without the FE technique for the double glide case (crystal orientation [1 1 2]) which corresponds to a deformation of the crystal without rotation of the lattice as specified by Tabourot et al. [30,44]. It was then used to reproduce stages II and III of the tensile curve of the [15 21 31] crystal orientation close to [1 1 2]. This first step reported initial values of some hardening parameters (K, y_c, $\mathbf{A}_{SH}$ and $\mathbf{A}_{LC}$). These values were then employed to simulate the tensile curves in single glide conditions extracted from the literature, considering the experimental sample dimensions and strain rates. Identification was achieved manually by adjusting the parameter values from one simulation to another until the tensile curve was correctly reproduced.

During the identification, a special attention was paid to the slip activity predicted by the model together with the different hardening stages. Depending on the crystal orientation and on the boundary conditions, some of the slip systems were not expected to be activated [45]. The hardening matrix coefficients were hence adjusted in order to reproduce both macroscopic tensile curves and microscopic slip system activities. Fig. 2 shows comparisons between predicted and experimental tensile curves for single glide orientations. The agreement between both experimental and predicted curves for each crystal orientation is satisfactory. In particular, the different hardening stages (the strain rate and the strain extent for each stage) are well reproduced by the model, except for the end of stage III where the difference between the predicted and experimental tensile curves is larger. This could be explained by the constant value of the annihilation distance, y_c, employed in the model for each crystal orientation. The parameter set obtained with the single glide orientations was then successfully validated on the multiple glide orientation (orientation [1 2 28]), as depicted in Fig. 2. Despite that this set of parameter values is not unique due to the manual identification procedure, the good agreement between the experimental tensile curves and the prediction of the model ensures that the deformation mechanisms of the single crystals were correctly captured. Moreover, a study of the sensitivity of the model on the parameter values showed that slight variations of parameter values do not deeply affect the microscopic and macroscopic mechanical responses of the Ni single crystals. This set of parameters can be hence used to investigate the size effects on the mechanical behavior of Ni single crystals.

Table 1 summarizes the different model parameter values identified for nickel. The physical meaning of each parameter can be found in the literature [27,28,5]. These latter are in the same order than those reported for Cu and Al [30,29,28], in agreement with their close stacking fault energy. It can be noticed that this set of parameters is different than the one identified by the authors in a previous study focused on the prediction of the mechanical behavior of small Ni polycrystals [5]. For single crystals, the identification of the hardening parameters, in particular the $\mathbf{A}_{ij}$ coefficients, is more sensitive than for polycrystals for which the effect of the coefficients is averaged by the several grain orientations. As a consequence, a new specific identification has been performed for this study focused on single crystals.

2.4. Investigation of the surface and size effects

In order to analyze the effect of dimensions on the mechanical behavior of Ni single crystals, two series of numerical tensile tests were performed. The first series corresponds to tensile tests with a crystal oriented for single glide, i.e. the orientation [3 10 32] depicted in Fig. 1(b), whereas a multiple glide condition (orientation [1 2 28], see Fig. 1(b)) was employed for the second series. For each series, different thickness values were used for simulations, the others dimensions being kept constant in the meantime. The initial crystal dimensions coincide to those of the crystals tested experimentally in the work of Venkatesan et al. [40]. The same geometry for the two series ensured that a difference of behavior between samples of both series with same dimensions must be caused by the crystal orientation. Table 2 summarizes the dimensions, Euler's angles and strain rate of the different numerical tensile tests performed. For each orientation, the reduced dimension (i.e. the thickness) was chosen such as it intersects the slip direction of the activated slip systems. For single glide orientations, the thickness corresponds to the dimension along $\mathbf{e}_x$ whereas it corresponds to $\mathbf{e}_y$ for the multiple glide one (see the crystallographic projections in Figs. 3(b) and 6(b)). The thickness values used for the simulations are (in mm): 10; 5; 3; 1; 0.5 and 0.25.

3. Results

3.1. Single slip conditions

The results of the tensile test obtained for the 5 mm × 5 mm section sample are represented in Fig. 3(a), together with the evolution

Table 1
Value of the material parameters of the strain gradient crystal plasticity model identified for nickel. The C_{ij} parameters correspond to the classical elastic moduli at the crystal level.

Parameter	$\mathbf{A}_{SH}$	$\mathbf{A}_{CP}$	$\mathbf{A}_{GJ}$	$\mathbf{A}_{CS}$	$\mathbf{A}_{HL}$	$\mathbf{A}_{LC}$	$\mathbf{H}_{SH}$	$\mathbf{H}_{CP}$	$\mathbf{H}_{GJ}$	$\mathbf{H}_{CS}$	$\mathbf{H}_{HL}$	$\mathbf{H}_{LC}$
Value	0.122	0.02	0.0915	0.0915	0.0915	0.0915	0.0	0.0	0.48	0.20	0.12	1
Origin	Id.	Id.	Id.	Id.	Id.	[29]	[29]	[29]	[29]	[29]	[29]	[29]

Parameter	K	C_{11}	C_{12}	C_{44}	G	$\dot{\gamma}_0$	m	b	G_0	y_c	R_s	R_e	ρ_{SSD_0}
Value	39	248 GPa	153 GPa	116 GPa	76 GPa	0.001 s^{-1}	0.02	0.25 nm	4.54×10^{-20} J	0.25 nm	5 nm	5 nm	Variable
Origin	Id.	[41]	[41]	[41]	[41]	[27]	[5]	[42]	[43]	Id.	Id.	Id.	Id.

Table 2
Summarize of the characteristics of the numerical tensile tests for Ni single crystals.

Series	Length (mm)	Width (mm)	Thickness (mm)	φ_1 (°)	ϕ (°)	φ_2 (°)	$\dot{\varepsilon}$ (s^{-1})
Single glide	20	5	From 10 to 0.25	18	17	15	0.002
Multiple glide	20	5	From 10 to 0.25	18	5	25	0.002

of the absolute value of the plastic shear rate of each activated slip system. Three hardening stages are depicted as expected for this orientation. For this single glide orientation four slip systems are initially favorably oriented with regard to the tensile direction: A3 (Schmid factor, $S_f \approx 0.5$), B4 ($S_f \approx 0.47$), D1 ($S_f \approx 0.36$) and B2 ($S_f \approx 0.33$) (the slip system notation corresponds to the one proposed by Franciosi et al. [46]). In stage I, only A3 is activated whereas in stage II and III, due to the crystal rotation associated to the plastic glide, the activity of A3 is reduced at the benefit of D1. For this orientation, the GND population is three times lower than the SSD one as no strain gradients induced by the mechanical test (for instance bending) or grain boundaries are introduced. The illustration of the different slip systems and the tensile direction is represented in the stereographic projection of the unstrained sample in Fig. 3(b).

The effect of the thickness on the tensile curves is depicted in Fig. 4. For this single glide orientation, the reduction in the thickness from 10 to 0.25 mm involves a strong increase of around 50 % in stage I extent in agreement with the experimental works of Fourie [6], Mughrabi [8,9] and Suzuki [47] on Cu single crystals. The hardening characteristics are also modified by a decrease in the thickness as described in Table 3. The values reported here have been obtained following the Kocks-Mecking formalism described in details in a previous paper [4]. In particular, the $(\tau\theta)_0$ parameter was obtained using the Kocks-Mecking plot of $\tau\theta$ vs τ (see [4]). This parameter value is related to the GND, to the initial dislocation structures and to the surface effect [4]. Concerning the stage I, it can be observed than the strain hardening rate θ_I decreases with a thickness reduction until a constant value for samples with thicknesses lower than 1 mm. For stage II, the strain hardening characteristics θ_{II} are virtually constant. The strain hardening mechanisms of stage I are hence strongly dimension dependent. For thicknesses lower than 1 mm, the mechanical behavior is independent of the dimensions.

Table 3
Hardening parameter values for the single crystals oriented in single glide as a function of the thickness. θ_i denotes the strain hardening rate, γ_i represents the critical strain for stage hardening activation and τ_i denotes the critical stress for the stage hardening activation, the subscript i represents the number of the strain hardening stage (i = I, II, III).

Thickness (mm)	θ_I (MPa)	θ_{II} (MPa)	γ_{I-II}	γ_{II-III}	$(\tau\theta)_0$ (MPa^2)
10	119	202	0.069	0.17	−1500
5	94	206	0.084	0.182	−2100
3	79	203	0.1	0.21	−2200
1	70	204	0.103	0.23	−2425
0.5	69.2	204	0.104	0.25	−2400
0.25	67.2	201	0.113	0.25	−2380

In order to investigate the mechanisms responsible for the effect of the thickness predicted by the model, the spatial distribution in three dimensions of the SSD dislocation density of the primary system A3 was plotted for the 5 mm × 5 mm cross section specimen in Fig. 5. This plot corresponds to the single crystal strained to a shear strain of 0.064 corresponding to the end of stage I. As seen in this figure, the SSD density distribution is not uniform with a strong gradient approximately perpendicular to the Burgers vector of the primary slip system A3, b_{A3}. Along this direction, the dislocation density is lower near the surfaces. In stage II, this dislocation density gradient is considerably reduced and the dislocation distribution becomes more homogeneous.

3.1.1. Multiple glide conditions

The results obtained for the 5 mm × 5 mm section sample oriented for multiple glide are represented in Fig. 6 in a way similar to the specimen oriented for single glide. The tensile curve presents only two hardening stages (i.e. II and III) as several glide systems are activated since the onset of plasticity. For this orientation, the

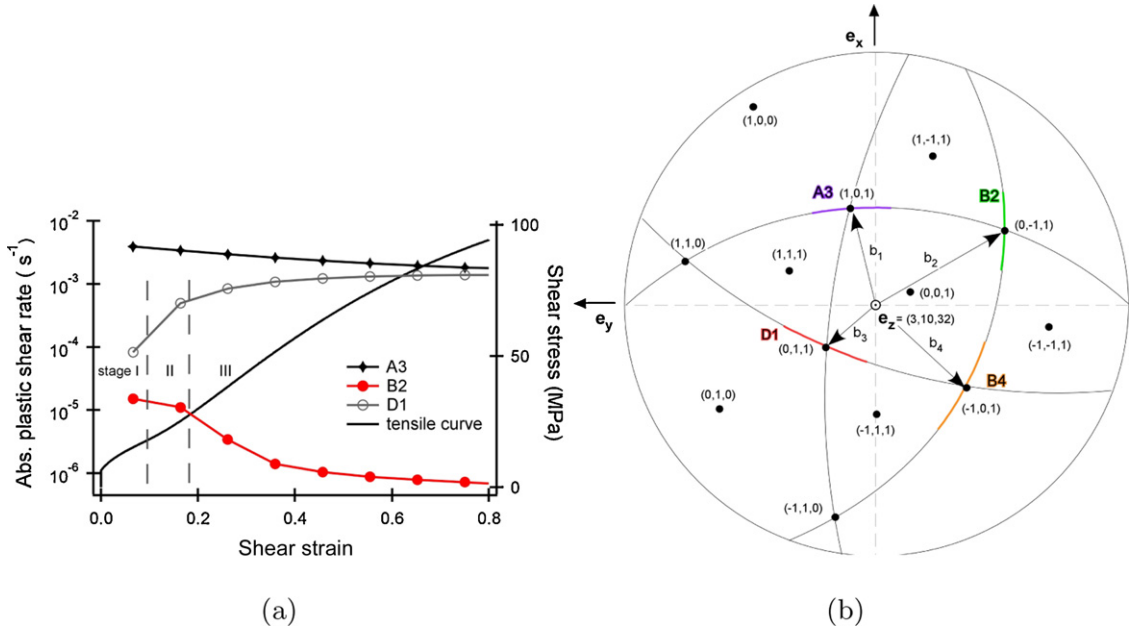

Fig. 3. Results of the simulated tensile test for the t = 5 mm specimen oriented for single glide: (a) tensile curve and evolution of the absolute value of the plastic shear rate of the activated slip systems and (b) stereographic projection of the unstrained sample, the $\mathbf{e}_x$, $\mathbf{e}_y$ and $\mathbf{e}_z$ express the reference system illustrated in Fig. 1 (a).

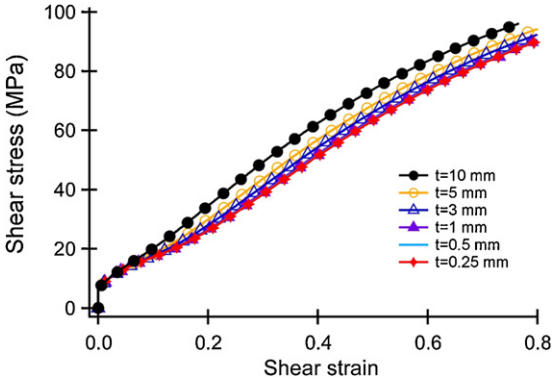

Fig. 4. Tensile curves for different thickness values for the single glide oriented specimen.

plastic strain is achieved by two main slip systems, A3 and D1. The others systems quickly stop to contribute to plasticity. As for the single glide orientation, the SSD density is significantly higher than the GND one. The slip directions of the activated slip systems and the tensile direction ($\mathbf{e}_z$) are illustrated in the stereographic projection of Fig. 6(b).

Considering the effect of the thickness on the flow stress, the difference between the thickest (t = 10 mm) and the thinnest (t = 0.25 mm) specimens is much less pronounced than for the single glide orientation (see Fig. 7). For the multiple glide orientation, the decrease in thickness affects the flow stress level after a few percents of strain whereas the extent of stage II remains unchanged. For a shear strain of 0.6, the shear stress difference is around 2 MPa between the thickest and the thinnest specimens as illustrated in the insert of Fig. 7. In comparison with single glide conditions, the hardening stages do not seem to depend on dimensions. As a consequence, the dimension effects appear to depend on the crystal orientation in agreement with the experimental work of Fourie [16].

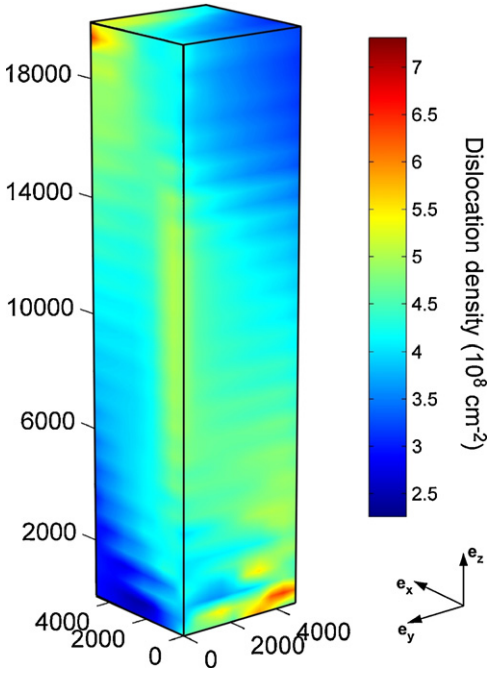

Fig. 5. 3D distribution of the statistically stored dislocations of the primary slip system A3 for the 5 mm × 5 mm cross section sample oriented for single glide. This plot is drawn in the undeformed configuration for a shear strain of 0.064 (the dimensions are expressed in μm).

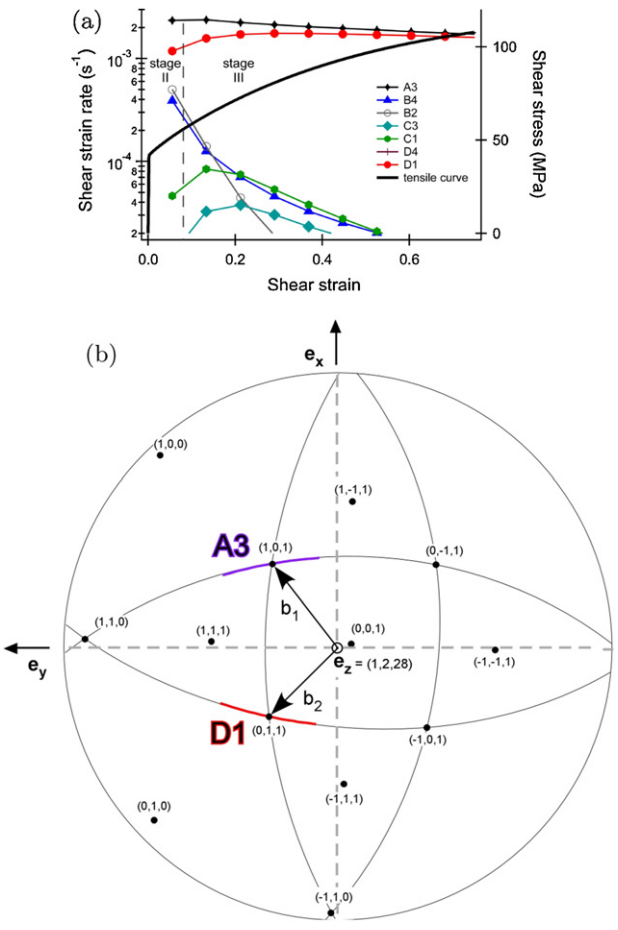

Fig. 6. Results of the simulated tensile test for the specimen oriented for multiple glide: (a) tensile curve and evolution of the absolute value of the plastic shear rate of the activated slip systems and (b) stereographic projection of the unstrained sample, the $\mathbf{e}_x$, $\mathbf{e}_y$ and $\mathbf{e}_z$ express the reference system illustrated in Fig. 1.

Fig. 8 represents the distribution of the SSD density of A3, in three dimensions for γ = 0.6, equivalent to stage III of hardening. Compared to Fig. 5 associated to single glide conditions, it can be observed that the single crystal oriented for multiple glide exhibits dislocation densities much more homogeneous. This homogeneity reflects the activation of the multiple glide systems and their

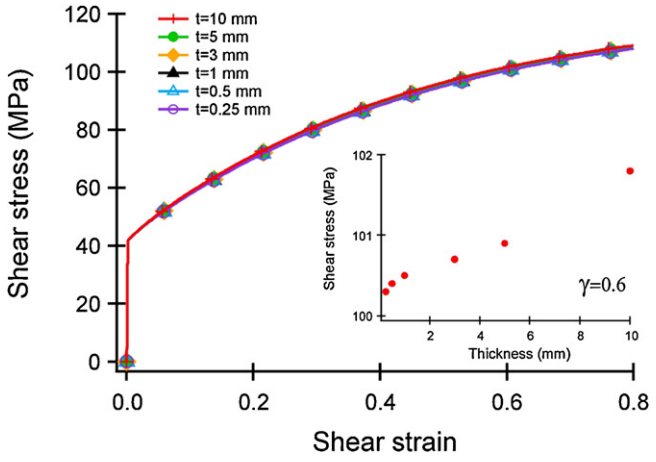

Fig. 7. Tensile curves for different thickness values for samples oriented for multiple glide.

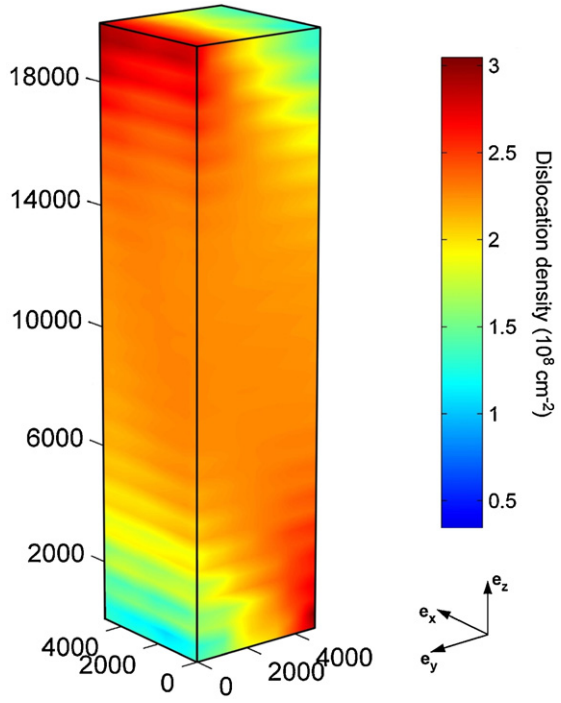

Fig. 8. 3D distribution of the statistically stored dislocations of the A3 system for the 5 mm × 5 mm cross section sample oriented for multiple glide. This plot is drawn in the undeformed configuration for a shear strain of 0.6 (dimensions are expressed in μm).

interactions. A weak gradient is still present perpendicular to the Burgers vector of A3.

4. Discussion

The previous results, provided by FE simulations using a strain gradient crystal plasticity model, highlight complex effects of a decrease in thickness on the mechanical behavior of nickel single crystal, in agreement with previous experimental studies [6–9,47]. Following these authors, the effect of dimensions is correlated to the formation of stress gradients between core and surface regions due to surface effects. In the following paragraphs, the results of simulations are discussed in terms of dislocation density gradient, mean free path of mobile dislocations and their interaction with surfaces. The objective is to determine the mechanisms responsible for the mechanical behavior modification with thickness decrease.

4.1. Stress gradient formation in single glide conditions

As illustrated in Table 3, the stage I of hardening for Ni single crystals oriented for single glide is strongly thickness dependent. Especially, the evolution of the parameter $(\tau_\theta)_0$ is worth noticing. As described in details in a previous paper [4], for pure f.c.c. materials, the evolution of dislocation density with strain is linked to two mechanisms, one linked to the contribution of the "forest dislocation" interactions involving an increase in the dislocation density and another one linked to annihilation events between dislocations (cross-slip or climb) reducing the quantity of dislocations. Depending on the material, other contributions may exist such as the initial dislocation structures of the material, the grain boundaries or free surfaces which can contribute in the production or annihilation of dislocations. The $(\tau_\theta)_0$ parameter is linked to these latter contributions: a positive value is related to the production of dislocations while a negative value traduces a dislocation density reduction [4]. In the case of the simulations performed in this work with single glide conditions, the initial dislocation density is the same (no initial dislocation structures are taken into account) and no grain boundaries can participate to strain hardening. The negative values obtained for simulations seem to be due to annihilation events occurring in the material. Following Mecking [48], a negative value for single crystals is associated to free surfaces which act as sinks for dislocations. This hypothesis seems to be in agreement with Fig. 5 which shows dislocation density gradients in stage I between core and surface regions of single crystals oriented for single glide. This gradient appears along a direction which is almost perpendicular to the Burgers vector of A3 slip system (b_{A3}).

Along b_{A3}, a dislocation density gradient is supposed to occur due to the emergence of dislocations across free surfaces. One can expect that dislocations located inside a layer with a thickness in the order of the mean free path of the dislocations, below the free surfaces, can escape across the latter. The model used for the simulations enables the computation of the mean free path of the different slip systems taking into account the interactions with the other systems. The maximum value reported by the simulations for A3 is around 60 μm which is in good agreement with experimental values reported by Huvier et al. for high purity Ni single crystals [49]. Hence, along b_{A3}, a dislocation density gradient may appear over distances of around 60 μm. Considering the large dimensions of the elements used in the simulations (1 mm × 1 mm × 1 mm, for computation time purpose) which are larger than the mean free path, the model is not able to reproduce this dislocation density gradient for large thicknesses. However, for $t = 0.25$ mm the mesh density is fine and no dislocation density gradient appears along b_{A3}.

The plastic shear activity of the primary slip system A3 is plotted in Fig. 9 in 3D. As seen in this figure, the slip activity of A3 is reduced near loading surfaces compared to the center of the specimen as the slip systems cannot emerge easily on these surfaces (node displacements along $\mathbf{e}_z$ restricted and dislocations cannot cross the loading surfaces). Moreover, GND develop in these zones in order to accommodate the plastic activity gradient. As the slip activity is reduced near the loading surfaces, the SSD density increases more slowly involving the stress gradient which is perpendicular to the A3 system. As a consequence, this dislocation density gradient is, in

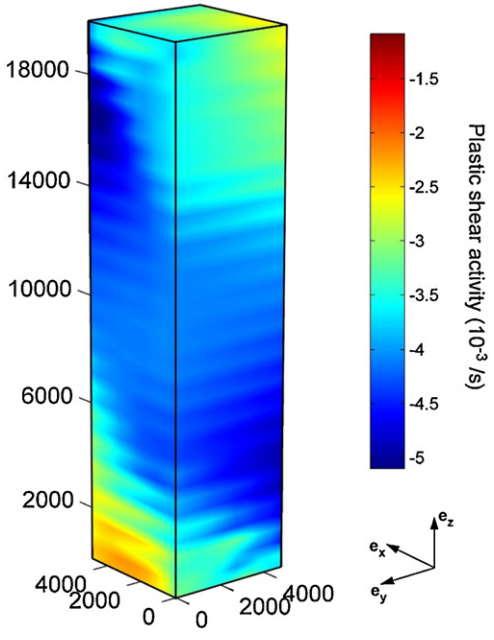

Fig. 9. Distribution of the plastic shear activity of the primary slip system A3 for single glide conditions for a shear strain of 0.064 (dimensions are expressed in μm).

the case of these simulations, not induced by surface effects but by the boundary conditions as suggested in a previous 2D numerical study by Kuroda and Tveergard [50].

The formation of these stress gradients associated to the SSD density distribution can explain the effect of the dimensions of the samples represented in Fig. 4 for the samples deformed in stage I. When sample thickness increases, the proportion of the crystal affected by the boundary conditions is larger and the GND necessary to accommodate the plastic activity gradient also increases. Due to this GND density rise, the strain hardening rate in stage I is increased, which, in turn, enhances the secondary slip system and shortens the macroscopic stage I of hardening as observed in Table 3. For the thinnest sample, the loading surfaces are considerably reduced which induces weak strain gradients homogenizing the mechanical behavior. In this case, plasticity can be accommodated by only one slip system for larger strains.

4.2. Role played by the crystal orientation

These mechanisms associated to the formation of plastic shear activity gradient due to boundary conditions can explain the role played by the crystallographic orientation on the effect of the thickness on the mechanical behavior of crystals oriented for multiple glide. As shown in Fig. 8, the difference of dislocation density between core and loading surfaces is considerably reduced compared to single glide orientation. For this multiple glide orientation, two principal slip systems are activated namely A3 and D1. The strain incompatibilities related to the boundary conditions near the loading surfaces are hence relaxed compare to single slip conditions. The dislocation density gradient observed Fig. 5 is then attenuated which, in turn, reduces the GND contribution, homogenizes the dislocation density and reduces the effect of dimensions. This phenomenon explains both the almost thickness independent stress values for crystals oriented in multiple glide and the constant values of hardening parameters in stage II for crystals oriented for single glide when two slip systems are activated. In this case, after stage I, the activation of the secondary slip system quickly homogenizes the dislocation density distribution.

4.3. Role played by a hard layer on surfaces

Following various authors [10–15], an oxide layer formation on the surfaces of the single crystals may modify the mechanical behavior for single glide orientation, especially during stage I, when large quantities of dislocations may escape through free surfaces. By modifying the boundary conditions for the GND on the lateral surfaces of the crystals, the model is able to reproduce the effect of a hard layer on the mechanical behavior. Fig. 10 represents the tensile curves of the single crystals oriented for single glide (same orientation as in the previous section) with both free and restricted surface conditions. For the 5 mm thickness, the hard layer introduction slightly modifies the tensile curve with a low decrease in stage I extent. However, if the thickness is further reduced, the differences between the predictions with the two boundary conditions increase. For the 0.25 mm thickness sample, stage I is completely deleted and the hardening rate is considerably increased in stage II if the hard layer is introduced. In this case, the results of the simulations show that the GND density contributes significantly to the plasticity and the secondary slip system is activated for a very low strain level whereas hardening is increased. As a consequence, the plastic strain is achieved by at least two slip systems which relaxed the stress gradients linked to the boundary conditions as explained for single crystals oriented for multiple glide.

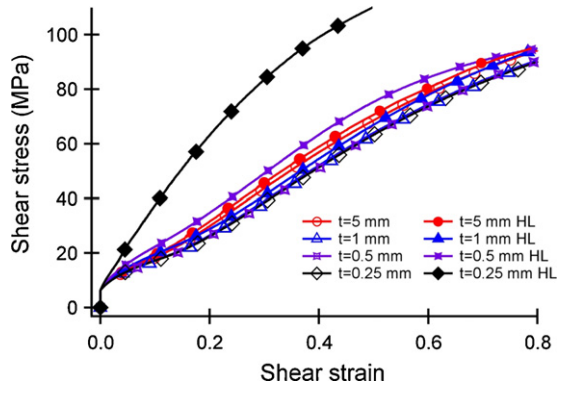

Fig. 10. Comparison between simulated tensile curves for sample oriented in single glide with free or constrained surfaces (HL for hard layer).

The effect of the thickness on the mechanical behavior of single crystals is then linked to two mechanisms, the first one associated to the boundary conditions related to the tensile machine and the second one is linked to the annihilation of dislocations on free surfaces. This second mechanism, not properly characterized by the simulations even for low thicknesses when the mesh density is fine, is nevertheless expected to be negligible compared to the first one as it may appear on distances lower than 60 μm. The boundary conditions are thus the most dominant mechanisms related to the size effect on the mechanical behavior of f.c.c. single crystals. These results reveal that the mechanisms of the size effect do not depend on the material as the same trend observed experimentally for Cu and Al are reproduced by the simulations for nickel.

5. Conclusions

The simulations performed with a strain gradient crystal plasticity model identified for nickel single crystals showed a complex effect of a thickness reduction on the mechanical behavior due to the boundary conditions. If these latter are characteristics of samples gripped in the tensile machine, the slip restriction near the loading surfaces involves a reduction in slip activity for single glide conditions. The dislocation density of the primary slip system is hence reduced near the edges which causes strong stress gradients whereas geometrically necessary dislocations appear to accommodate the difference of slip activity. For larger thicknesses, the increase in GND density promotes double slip activity, decreases the strain extent of the stage I hardening and increases the strain hardening rate. For multiple glide conditions, the strain incompatibilities near the loading edges are relaxed, involving homogeneous dislocation density and almost thickness independent mechanical behavior. The effect of surfaces does not seem to influence the mechanical behavior except in the case of passivated surfaces. In this case, the GND increase promotes multislip conditions which, for low thicknesses, completely delete stage I of hardening.

The results of this study show that the mechanisms based on surface effects enounced in previous experimental studies to explain the dimension effect for the "smaller is softer" trend on the mechanical behavior of single crystals, may be partially erroneous as the important contribution of the boundary conditions was not considered by these authors [6–9,47].

Acknowledgements

The authors acknowledge the Interuniversity Attraction Poles Program – Belgian State – Belgian Science Policy (Contract P6/24) for the financial support. The Belgian Fund for Scientific Research FRS-FNRS is also acknowledged.

References

[1] M. Geiger, M. Kleiner, R. Eckstein, R. Tiesler, U. Engel, Ann. CIRP 50 (2001) 445–462.
[2] P. Janssen, T. de Keijser, M. Geers, Mater. Sci. Eng. A 419 (2006) 238–248.
[3] S. Miyazaki, K. Shibata, H. Fujita, Acta Metall. 27 (1979) 855–862.
[4] C. Keller, E. Hug, X. Feaugas, Int. J. Plast. 27 (2011) 635–654.
[5] C. Keller, E. Hug, A.M. Habraken, L. Duchene, Int. J. Plast. 29 (2012) 155–172.
[6] J. Fourie, Philos. Mag. 17 (1967) 735–756.
[7] J. Fourie, Philos. Mag. 21 (1970) 977–985.
[8] H. Mughrabi, Phys. Status Solidi 39 (1970) 317–327.
[9] H. Mughrabi, Phys. Status Solidi 44 (1971) 391–402.
[10] S. Kitajima, H. Oasa, H. Kaieda, Trans. Jpn. Inst. Metals 8 (1967) 185–190.
[11] S. Kitajima, H. Oasa, H. Kaieda, Trans. Jpn. Inst. Metals 10 (1968) 12–16.
[12] I. Kramer, Trans. Metall. Soc. AIME 227 (1963) 1003–1010.
[13] I. Kramer, Trans. Metall. Soc. AIME 239 (1967) 1754–1758.
[14] Z. Basinski, in: J.F.R.M. Latanision (Ed.), Surface Effects in Crystal Plasticity, Nato Advanced Study Institutes Series, 1977, pp. 66–88.
[15] F. Nabarro, in: J.F.R.M. Latanision (Ed.), Surface effects in Crystal Plasticity, Nato Advanced Study Institutes Series, 1977, pp. 66–88.
[16] J. Fourie, Proceedings of the 7th International Conference on Strength of Metals and Alloys, Pergamon Press, 1986, pp. 99–104.
[17] C. Han, A. Hartmaier, H. Gao, Y. Huang, Mater. Sci. Eng. A 415 (2006) 225–233.
[18] N. Fleck, G. Muller, M. Ashby, J. Hutchinson, Acta Metall. Mater. 42 (1994) 475–487.
[19] J. Stolken, A. Evans, Acta Mater. 46 (1998) 5109–5115.
[20] J.Y. Shu, N.A. Fleck, E.V. der Giessen, A. Needleman, J. Mech. Phys. Solids 49 (2001) 1361–1395.
[21] L. Nicola, E.V. der Giessen, A. Needleman, Thin Solid Films 479 (2005) 329–338.
[22] T.A. Parthasarathy, S.I. Rao, D.M. Dimiduk, M.D. Uchic, D.R. Trinkle, Scripta Mater. 56 (2007) 313–316.
[23] J.R. Greer, W.C. Oliver, W.D. Nix, Acta Mater. 53 (2005) 1821–1830.
[24] D. Dimiduk, M. Uchic, T. Parthasarathy, Acta Mater. 53 (2005) 4065–4077.
[25] D. Kiener, W. Grosinger, G. Dehm, R. Pippan, Acta Mater. 56 (2008) 580–592.
[26] H. Espinosa, B. Prorok, B. Peng, J. Mech. Phys. Solids 52 (2004) 667–689.
[27] L. Evers, W. Brekelmans, M. Geers, J. Mech. Phys. Solids 52 (2004) 2379–2401.
[28] L. Evers, W. Brekelmans, M. Geers, Int. J. Solids Struct. 41 (2004) 5209–5230.
[29] A. Arsenlis, D.M. Parks, J. Mech. Phys. Solids 50 (2002) 1979–2009.
[30] L. Tabourot, M. Fivel, E. Rauch, Mater. Sci. Eng. A 234–236 (1997) 639–642.
[31] A. Thompson, Work Hardening in Tension, Fatigue, American Institute of Mining, Metallurgical, Petroleum Engineers, 1977, pp. 89–126.
[32] Z. Yao, R. Schublin, M. Victoria, J. Nucl. Mater. 307–311 (2002) 374–379.
[33] H. Kronmuller, Z. Phys. 154 (1959) 574–600.
[34] L. Hollang, E. Hieckmann, D. Brunner, C. Holste, W. Skrotzki, Mater. Sci. Eng. A 424 (2006) 138–153.
[35] M. Hecker, E. Thiele, C. Holste, Acta Mater. 50 (2002) 2357–2365.
[36] P. Haasen, Philos. Mag. 8 (1958) 384–418.
[37] R. Latanision, R. Staehle, Acta Metall. 17 (1969) 307–319.
[38] E. Kondrat'ev, A. Pets, Russ. Phys. J. 02 (1972) 242–244.
[39] G. Girardin, D. Delafosse, Scripta Mater. 51 (12) (2004) 1177–1181.
[40] P. Venkatesan, D. Beshers, Metall. Trans. 1 (1970) 1780–1783.
[41] B. Landolt, Landolt-Bornstein Tables, vol. III, Springer-Verlag, 1966.
[42] C. Keller, Ph.D. Thesis, Universite de Caen/Basse-Normandie, France, 2009.
[43] W. Ashmawi, M. Zikry, J. Comput.-Aided Mater. 7 (2000) 55–62.
[44] L. Tabourot, Habilitation á diriger des recherches, Université de Savoie, France, 2001.
[45] B. Jaoul, Etude de la plasticite et application aux metaux, Dunod, 1965.
[46] P. Franciosi, M. Berveiller, A. Zaoui, Acta Metall. 28 (1980) 273–283.
[47] H. Suzuki, S. Ikeda, S. Takeushi, J. Phys. Soc. Jpn. 11 (1956) 382–393.
[48] H. Mecking, Work Hardening in Tension, Fatigue, American Institute of Mining, Metallurgical, Petroleum Engineers, 1977, pp. 66–88.
[49] C. Huvier, E. Conforto, H.E. Alami, D. Delafosse, X. Feaugas, IOP Conf. Series: Materials Science and Engineering, IOP publishing, 2009, pp. 1–6.
[50] M. Kuroda, V. Tveergard, Int. J. Solids Struct. 46 (2009) 4396–4408.